

# An Ensemble Framework for Explainable Geospatial Machine Learning Models

Lingbo Liu<sup>1,2\*</sup>

<sup>1</sup>School of Urban Design, Wuhan University; Wuhan, 430072, China.

<sup>2</sup>Center for Geographic Analysis, Harvard University; Cambridge, 02138, USA.

\*Corresponding author. Email: lingboliu@fas.harvard.edu.

**Abstract:** Analyzing spatial varying effect is pivotal in geographic analysis. Yet, accurately capturing and interpreting this variability is challenging due to the complexity and non-linearity of geospatial data. Herein, we introduce an integrated framework that merges local spatial weighting scheme, Explainable Artificial Intelligence (XAI), and cutting-edge machine learning technologies to bridge the gap between traditional geographic analysis models and general machine learning approaches. Through tests on synthetic datasets, this framework is verified to enhance the interpretability and accuracy of predictions in both geographic regression and classification by elucidating spatial variability. It significantly boosts prediction precision, offering a novel approach to understanding spatial phenomena.

Keywords: Explainable Artificial Intelligence (XAI). GeoAI, Machine Learning, Spatial Varying, Geographically Weighted Models

# 1 Introduction

The relationships between things can vary significantly across different spatial or geographical contexts, a phenomenon that manifests in various spatial events such as the disparate impacts of pandemics[1], the dynamics of poverty distribution[2], fluctuations in housing prices[3], etc. By optimizing spatial analysis methods, we can enhance the accuracy of predictions, improve the interpretability of models, and make more effective spatial decisions or interventions[4]. Nonetheless, the inherent complexity of spatial data and the potential for nonlinear relationships pose challenges to enhancing interpretability through traditional spatial analysis techniques.[5].

In terms of models for analyzing spatial varying effects such as spatial filtering models[6-8] and spatial Bayes models [9], Geographically Weighted Regression (GWR) and Multiscale Geographically Weighted Regression (MGWR) stand out for their application of local spatial weighting schemes, which are instrumental in capturing spatial features more accurately[10, 11]. These linear regression-based approaches, however, encounter significant hurdles in decoding complex spatial phenomena (Figure 1). Various Geographically Weighted (GW) models have been developed to tackle issues such as multicollinearity [12, 13] and to extend the utility of GW models to classification tasks[14-17]. The evolution of artificial intelligence (AI) methodologies, including Artificial Neural Networks (ANN) [18], Graph Neural Networks (GNN) [19, 20], and Convolution Neural Networks (CNN) [21], has introduced novel ways to mitigate uncertainties around spatial proximity and weighting kernels in GW models. Despite these advancements in marrying geospatial models with AI, challenges remain in addressing nonlinear correlations and deciphering underlying spatial mechanisms.

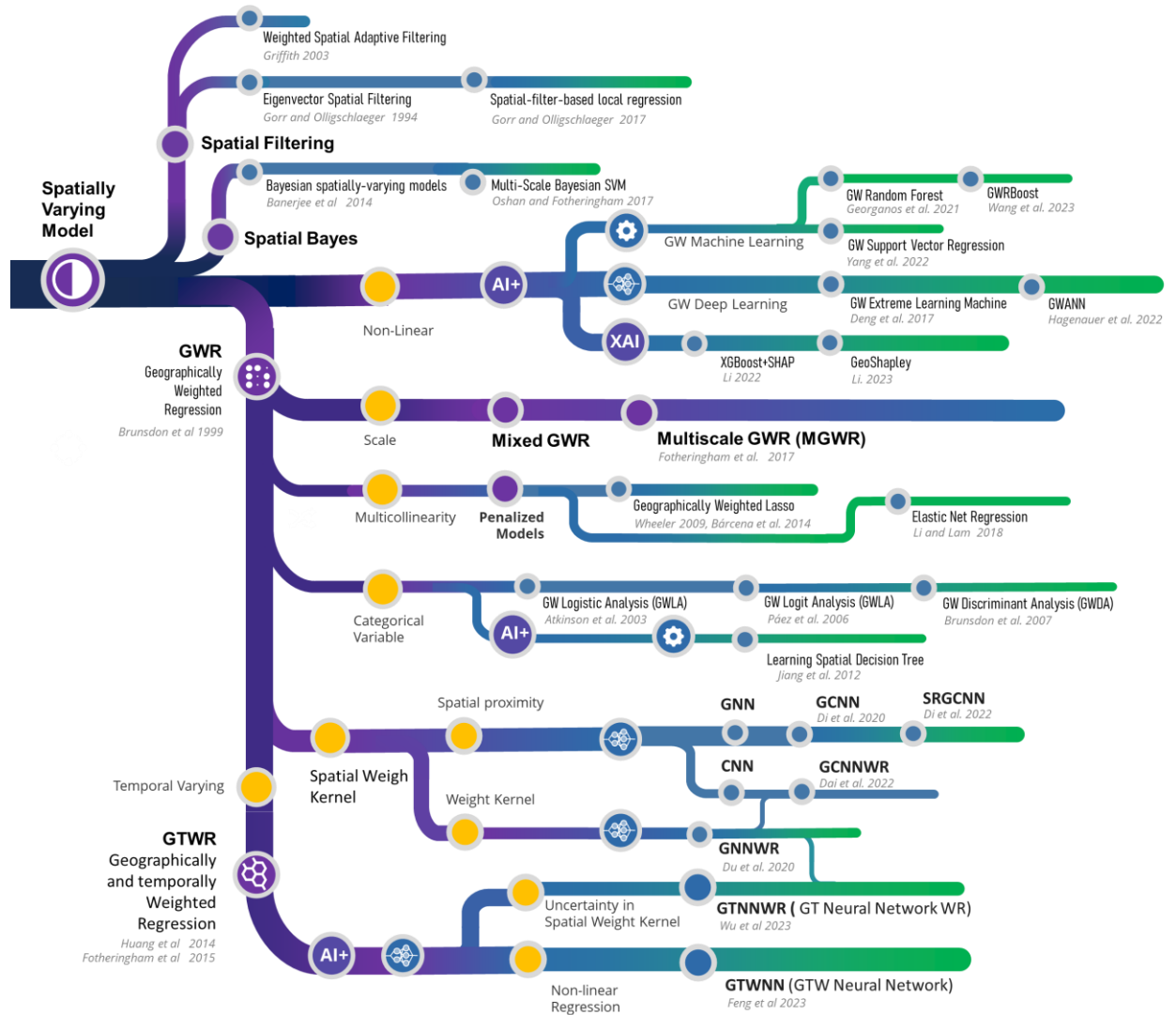


Figure 1: The evolution tree of models for spatial varying effect.

The burgeoning interest in Geospatial AI (GeoAI) and the integration of explicit geographical relationships with AI models herald an important trend towards improving predictions regarding nonlinear relationships and complex spatial phenomena[22-24]. This trend bifurcates into two categories[25, 26]. One integrates spatial weighting scheme into AI models, such as GW Support Vector Regression[27], GWANN[28], and GW Extreme Learning Machine[29], GW Random Forest[30, 31], ANN for Geographically and temporally weighted regression(GTWR) [32, 33]. These models focus predominantly on prediction with less emphasis on interpretability. Moreover, these models often concentrate on a single algorithm and are implemented in various programming languages, which hampers their replicability and the ability to perform

stable comparisons[34]. The other category involves explainable AI (XAI) algorithms, such as LIME[35], SHAP[36], or Feature Importance[37] in tree models, which offer valuable tools for demystifying the "black box" of machine learning algorithms, enhancing geographic analysis from an interpretability perspective[38, 39]. Recently, an ensemble method named GeoShapley was proposed to offer a universal analytical method for machine learning. It provides spatial varying coefficients particularly in assessing the contribution of geographical coordinates to geographic models[40]. However, the direct interpretation results from SHAP or Shapley values often contain substantial noise, necessitating spatial interpolation through GWR to refine the analysis. This requirement presents a challenge for the direct application of GeoShapley, indicating a need for improved methodologies that can leverage the strengths of XAI.

Therefore, we propose an integrated, universally explainable geospatial machine learning ensemble framework that builds upon the foundational assumptions of geographic weighting while incorporating explainable AI technologies. This framework not only leverages the spatial feature capture of GWR and the computational efficiency of AI models but also bolsters model interpretability through XAI, addressing the shortcomings of conventional approaches. Our multi-model testing on synthetic datasets illustrates the framework's enhanced capability to accurately capture and elucidate spatial variability, thereby providing robust support for decision-making and predictive modeling across various spatial studies. This research not only underscores the potential of this integrated framework in augmenting prediction accuracy and applicability but also presents a versatile approach capable of addressing a wide spectrum of spatial variability challenges, making it readily applicable to practical spatial analysis scenarios.

## 2 Data and Methodology

### 2.1 Data

systematic approach was employed to generate a synthetic dataset designed to simulate complex spatial relationships, leveraging a 30x30 spatial grid as the foundational structure. Each point within this grid was assigned four independent random variables, each drawn from a standard normal distribution  $\mathbf{N}(0,1)$ . Additionally, an error term ( $\epsilon$ ) was introduced to each point, originating from a normal distribution with a mean of zero and a standard deviation of 0.5, to emulate observational errors commonly encountered in empirical data.

To incorporate spatial variability into the dataset, four distinct spatial gradient patterns were devised: a linear gradient, set at a 45-degree angle to create a continuous variable across the 0 to 1 range ( $\beta_{\text{linear}}$ ); a circular gradient centered within the grid to simulate radially diminishing effects ( $\beta_{\text{circular}}$ ); a cosine gradient to introduce regular spatial fluctuations ( $\beta_{\text{cosine}}$ ); and a kernel density gradient, employing Gaussian kernels placed at strategic locations to simulate localized clustering phenomena ( $\beta_{\text{polycentric}}$ ). These gradients collectively aim to mimic the diverse spatial effects observed in real-world data.

To ensure model training stability and facilitate the observability of model validation, all spatial gradient variables underwent normalization to a uniform range of 0 to 5. This normalization process was critical for maintaining variable consistency across the dataset.

$$Y_0 = \beta_{\text{linear}}X_1 + \beta_{\text{circular}}X_2 + \beta_{\text{cosine}}X_3 + \beta_{\text{polycentric}}X_4 \quad (1)$$

$$Y = \beta_{\text{linear}}X_1 + \beta_{\text{circular}}X_2 + \beta_{\text{cosine}}X_3^2 + \beta_{\text{polycentric}}X_4^3 \quad (2)$$

Building upon the simulated spatial variability, a linear response variable ( $Y_0$ ) was constructed as per Equation 1. This was achieved through a linear combination of the spatial gradient variables and the random variables, incorporating the error term to introduce variability. Furthermore, a nonlinear response variable ( $Y$ ) was formulated to

capture more complex spatial dynamics. This variable integrates the spatial gradient variables and the random variables in a similar fashion but introduces nonlinearity through the transformation of  $X_3$  and  $X_4$ , which are squared and cubed, respectively, as detailed in Equation 2. These transformations were specifically chosen to enhance the representation of complex spatial relationships within the model.

The example data and Google Colab notebook are available at <https://github.com/UrbanGISer/XGeoML>. The XGeoML can be installed via PYPI, <https://pypi.org/project/XGeoML/0.1.4/>.

## 2.2 Methodology

The proposed Explainable Geospatial Machine Learning (XGeoML) model integrates the spatial weighting principles from GWR with machine learning technologies to enhance the model's responsiveness to local spatial variability and predictive accuracy. By incorporating spatial weights into the model design, XGeoML adeptly captures the complexity and non-linearity inherent in spatial data (Figure 2).

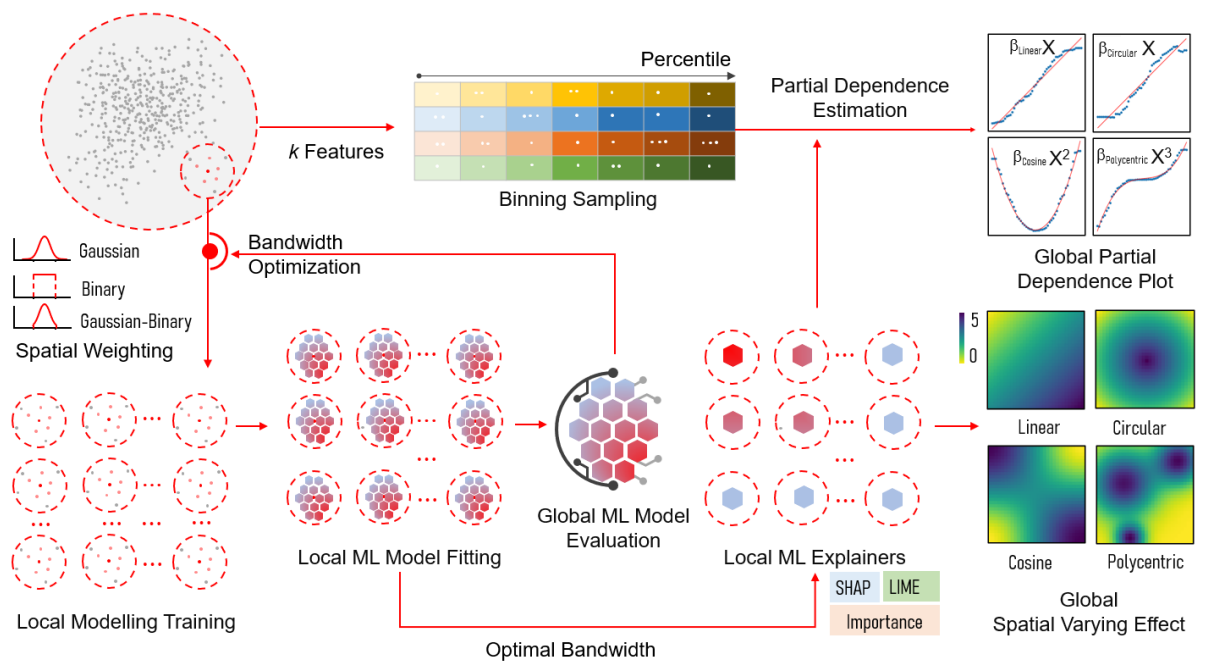


Figure 2: Workflow of the Explainable Geospatial Machine Learning (XGeoML)

Model. a. Initial Bandwidth and Weighting Scheme: Select default bandwidth and appropriate spatial weighting scheme; b. Local Model Construction & Evaluation: Construct local models for each point; use leave-one-out cross-validation for machine learning training, prediction, and evaluation; c. Optimal Bandwidth Search: Iterate over bandwidths to find the optimal setting for maximum model performance; d. Integration & Explanation: Combine the optimal bandwidth with the machine learning model; apply SHAP, LIME, and Feature Importance for interpretable spatial variability coefficients. E. Partial Dependency Estimation: Use percentile binning sampling on  $k$  features for partial dependency estimations with the trained model.

### 2.2.1 Integration Foundation for Spatial Weighting Scheme and Machine Learning

The foundation of this XgeoML model is explained through mathematical formulations. In the framework of Ordinary Least Squares (OLS), the objective is to identify coefficients  $\beta$  that minimize the sum of squared errors. The Geographically Weighted Regression (GWR) model, however, adjusts for each local point  $i$  based on surrounding points and their spatial weights  $w_i$ , utilizing weighted least squares to depict spatial variability (Equation 3). This process effectively entails multiplying both explanatory and response variables by the square root of their spatial weights before conducting a standard OLS analysis. We propose that similarly processing the explanatory and response variables within a machine learning model—by multiplying them by the square root of their spatial weights—can more precisely model spatial variations, thereby improving the accuracy and stability of predictions.

$$S_W(\beta) = \sum_{i=1}^n w_i (y_i - x_i^T \beta)^2 \quad ; \quad S_W(\beta) = \sum_{i=1}^n \left( \sqrt{w_i} y_i - \sqrt{w_i} x_i^T \beta \right)^2 \quad (3)$$

### 2.2.2 Bandwidth and Spatial Weighting Kernel Selection

The choice of bandwidth and kernel significantly influences model performance in geospatial machine learning models. We explored three different kernel modes: Gaussian, Binary, and Gaussian Binary, each affecting the distribution of spatial

weights and thus the model's predictive capacity and interpretability.

Gaussian Kernel: Utilizes a continuous Gaussian function to allocate spatial weights, with weights decreasing as distance increases, given by:

$$w_i = \exp\left(-\frac{d_i^2}{2\sigma^2}\right) \quad (4)$$

where  $d_i$  represents the distance from the target point to other points, and  $\sigma$  is the bandwidth parameter controlling the rate of spatial weight decay.

Binary Kernel: Assigns a weight of 1 to points within the bandwidth range and 0 to points outside. This method is straightforward, ensuring that only points within a certain distance from the target point contribute to the prediction.

Gaussian Binary Kernel: Combines the characteristics of Gaussian and Binary kernels, allocating weights according to a Gaussian distribution within the bandwidth and 0 outside.

### 2.2.3 Local Machine Learning Training and Spatial Interpretability

Assuming that an independent machine learning model is constructed for each observation point simplifies the model training process, thereby avoiding complex hyperparameter optimization. In experiments, we utilized default parameter configurations of regression models from the scikit-learn Python packages and conducted model training and validation using leave-one-out (LOO) cross-validation.

Its interpretability is enhanced through the integration of explanatory tools such as Local Interpretable Model-agnostic Explanations (LIME), SHapley Additive exPlanations (SHAP) for general models and Feature Importance in tree-based models.

LIME offers explanations by approximating the local decision boundary of complex models, with its formula represented as:

$$LIME(x) = \arg \min_{g \in G} L(f, g, \pi_x) + \Omega(g) \quad (5)$$

where  $f$  is the original model,  $g$  is a simplified model (e.g., a linear model),  $\pi_x$  is a function measuring the local neighborhood,  $L$  is a loss function that measures how well  $g$  approximates  $f$  in the neighborhood of  $x$ , and  $\Omega$  is a complexity penalty.



SHAP assigns a contribution value to each feature based on the Shapley value from game theory, with the formula:

$$\phi_j = \sum_{S \subseteq N \setminus \{j\}} \frac{|S|! (|N| - |S| - 1)!}{|N|} [f(S \cup \{j\}) - f(S)] \quad (6)$$

where  $N$  is the set of all features,  $S$  is a subset of features excluding feature  $j$ ,  $f(S)$  is the prediction of the model with feature set  $S$ , and  $\phi_j$  is the Shapley value of feature  $j$ , indicating its average contribution to the model's prediction.

For tree-based models, such as random forests and gradient boosting trees, Feature Importance is commonly used to assess the importance of each feature in model predictions. Feature importance can be calculated based on the frequency of feature usage in tree splits or the purity gain from the splits, with a common calculation method being:

$$Importance(x) = \sum_{t \in T} \Delta \text{purity}(t) \quad (7)$$

where  $T$  is the set of all tree nodes that split on feature  $x$ , and  $\Delta \text{purity}(t)$  is the purity gain from splitting at node  $t$ .

For partial dependence estimation, a binning sampling method is employed. By dividing each feature variable into uniform intervals and selecting sample points within each interval, we efficiently estimate the model's partial dependence on various features with reduced computational cost.

#### 2.2.4 Model Comparison and Evaluation

Using a synthetic dataset, we evaluated and compared the performance of various geospatial models, including GWR, MGWR, and GeoShapley. Our comparative analysis extended to assessing the prediction accuracy ( $R^2$ ) of different models, the correlation between spatial variability coefficients and the actual model, the performance of XGeoML model under various bandwidth forms and weighting methods, the variability in interpretability models across different bandwidths, and the

performance of all machine learning models from the scikit-learn package using uniform parameter settings.

These comparisons delved into the models' proficiency in capturing and elucidating spatial data variability and their capability to discern the structure and dynamics inherent in spatial data. This holistic approach not only highlighted each model's strengths and weaknesses in predicting and understanding spatial phenomena but also shed light on the efficacy of XGeoML in leveraging spatial weighting principles and machine learning to enhance both predictive accuracy and model interpretability.

### **3 General Comparison of Linear Model and Nonlinear Model**

#### ***3.1 Linear Model***

Within the context of linear models, GWR and MGWR accurately and stably capture the spatial varying coefficients of the explanatory variables in the synthetic data (Figure 3). Conversely, the GeoShapley model, developed on the Multilayer Perceptron (MLP) neural network framework, exhibits deficiencies in accurately determining the original spatial variability coefficients, attributed mainly to the substantial presence of noise within the model. Despite this, most predictive values persistently align with the original spatial variability coefficients. Remarkably, post-application of GWR for smoothing the initial dataset, GeoShapley's outcomes can emulate the spatial patterns exhibited by MGWR, enhancing predictive accuracy. This adaptation, however, may diminish the novel allure of employing GeoShapley.

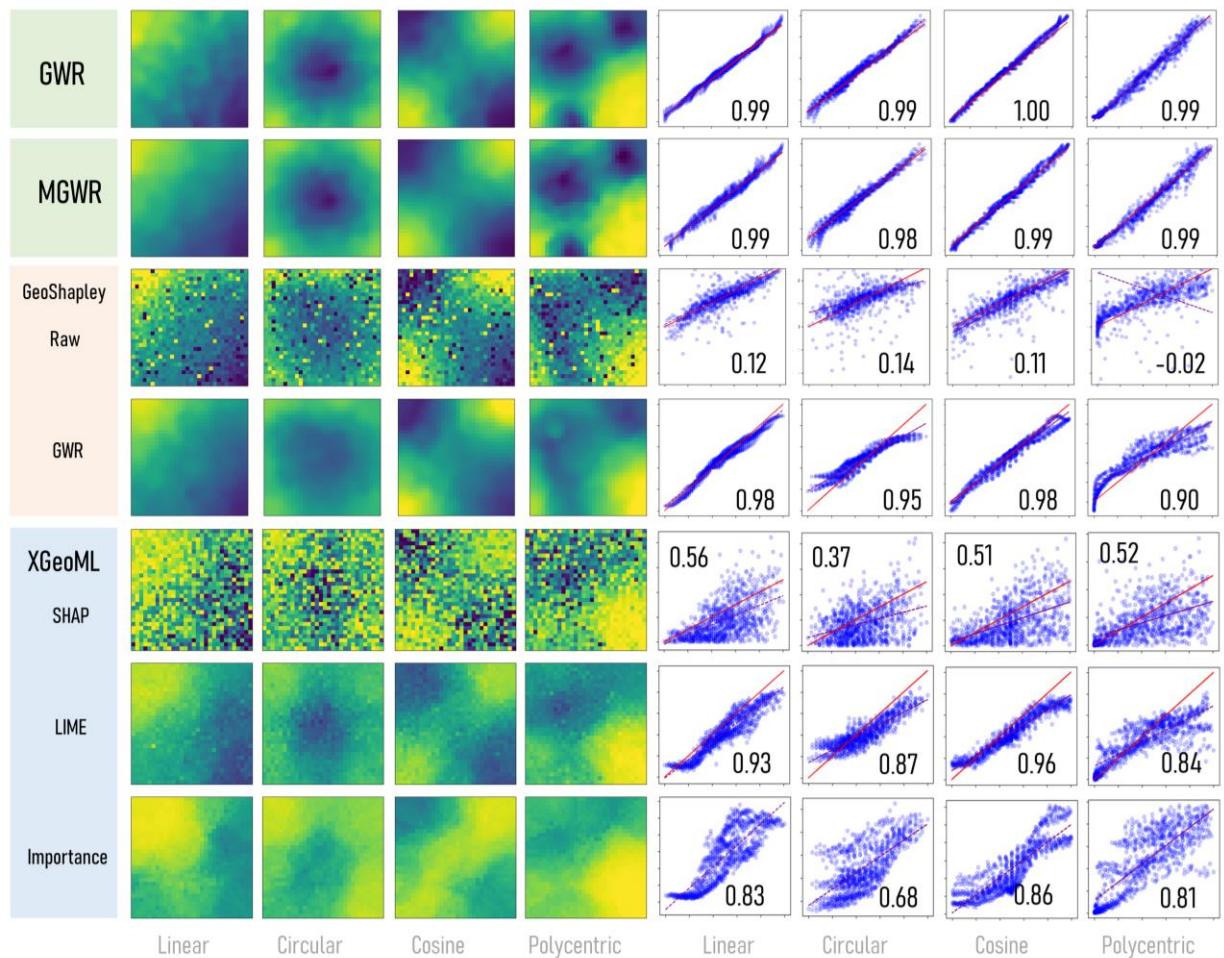
The XGeoML model, which utilizes an adaptive bandwidth approach by selecting the nearest 150 data points, and integrates an ensemble model, Gradient Boosting Regressor, with all the three different explainability models. The results in Table 1 show that LIME outperforms in terms of accuracy, followed by Importance, while SHAP coefficients are relatively lower. Overall, this indicates that XGeoML exhibits exceptional performance in processing linear models, especially in terms of

computational efficiency. Conducted on the same Google Colab platform, XGeoML's execution spanned 142 seconds, in contrast to GeoShapley's 42 seconds, facilitated by HyperOpt's automated hyperparameter optimization for 10-fold cross-validation. The spatial varying effect's model explanation phase necessitated 540 seconds. Noteworthy, despite leveraging sklearn package's default parameter configurations, XGeoML secures commendable results, accentuating the pivotal contribution of spatial weighting towards augmenting model performance.

Table 1. Model accuracy based on  $R^2$

OLS	GWR	MGWR	GeoShapley*		XGeoML- GBR-Fixed bandwidth	
			MLP	GBR	Binary	Gaussian Binary
0.37	0.70	0.81	0.76	0.75	0.75	0.66

\*MLP : Train 0.97, Test 0.51 , GBR , Train: 0.96, Test:0.48



(a)

(b)

Figure 3: Model comparison based on linear equations. (a) visualizes the spatial variability coefficients, (b) depicts the correlation between predicted coefficients and coefficients in the true model. Axes are scaled 0-5, barring GeoShapley's raw coefficients on the Y-axis, spanning -4 to 4, and XGeoML's Importance on the Y-axis, ranging 0-1. The red line,  $y=x$ , illustrates the ideal scenario where predicted values should equal the true values. Each column represents the target coefficients in the true model, with each row corresponding to different models.

### ***3.2 Nonlinear Model***

Within the context of linear models, All models accurately and stably capture the spatial varying coefficients of the explanatory variables in the synthetic data (Figure S1). While applied for of nonlinear model, the XGeoML model achieved an  $R^2$  value of 0.95 on the training set and 0.75 on the test set. Although this performance is slightly below the 0.81  $R^2$  value of the MGWR model, it surpasses the GeoShapley model, which exhibited an impressive  $R^2$  of 0.97 in the training set but experienced a substantial drop to an  $R^2$  of only 0.50 in the test set. Moreover, when choosing a fixed bandwidth, the XGeoML 's binary weight-based  $R^2$  performance exceeded that of the Gaussian binary weights, highlighting the crucial impact of spatial weights on model performance.

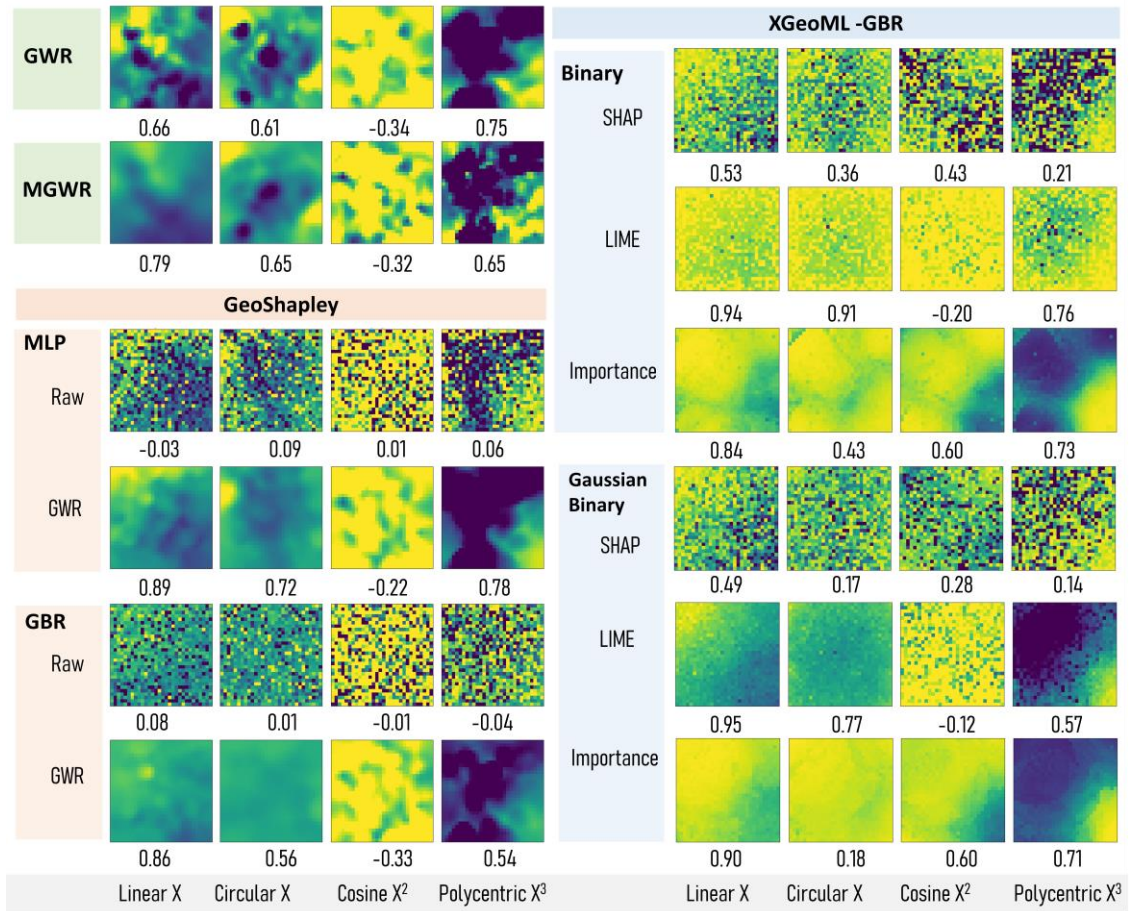
However, the visualization of spatial variability coefficients in Figure 4(a) reveals the XGeoML model's prominence. The result shows that GWR, MGWR, and GeoShapley models underperformed in capturing spatial variability coefficients related to the interaction between cosine spatial coefficients and the square of variables, whereas the XGeoML model effectively captured these changes. Although the GeoShapley model made some progress in capturing monotonic relationships (such as  $x$  and  $x$  cubed) through optimization of the GWR model, it did not exhibit competitive performance in capturing the interaction between cosine spatial variability features and the square of variables, whether based on MLP or GBR. This outcome emphasizes the challenges

models face when dealing with complex spatial changes and non-monotonic variable interactions.

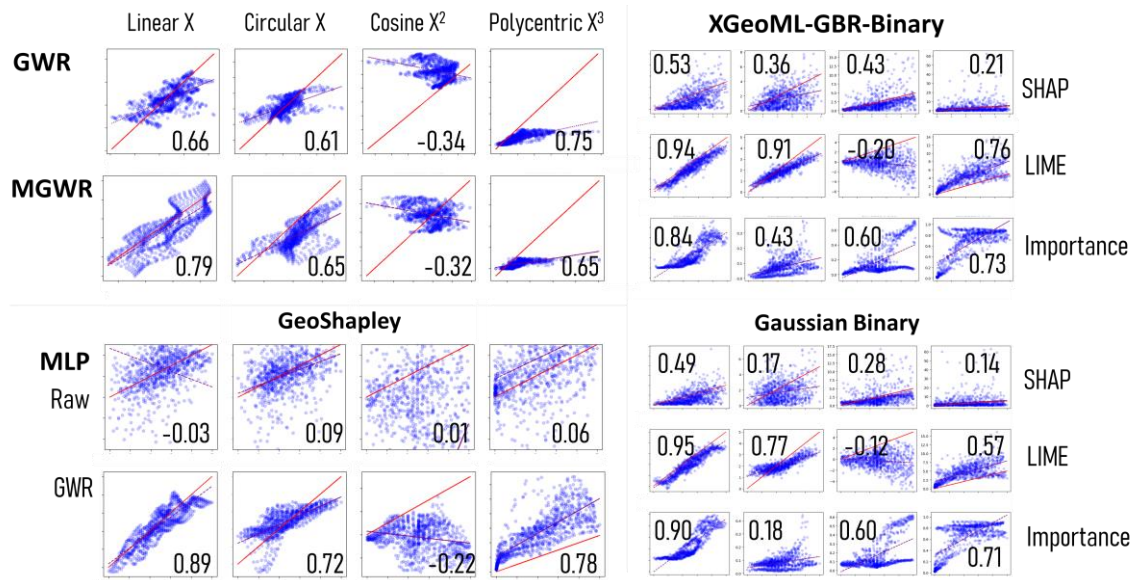
The scatter plot for correlation in Figure 4(b) verifies the interpretative capability provided by the explainers of SHAP and Importance which showed positive correlations in both binary or Gaussian binary weighting method. Notably, the LIME analysis outperformed GWR, MGWR, and GeoShapley on three other coefficients based on monotonous relationships. Although SHAP showed positive correlation relative to LIME, its weaker influence suggests potential for improvement in nonlinear model performance and possibly explains GeoShapley's interpretability shortcomings. The XGeoML model's Importance analysis was particularly effective in capturing changes in cosine spatial variability and the square of variables  $x$ . This highlights the XGeoML model's comprehensive advantage in interpretability and accuracy under diverse and complex conditions.

The results of partial dependency estimations are presented in Figure 5. Both GeoShapley and XGeoML accurately captured the variation patterns of the four explanatory variables, particularly the quadratic function of  $x^3$  and the cubic function of  $x^4$ .





(a)



(b)

Figure 4: Model comparison based on nonlinear equations. (a) visualizes the spatial variability coefficients, (b) depicts the correlation between predicted coefficients and

coefficients in the true model. The red line,  $y=x$ , illustrates the ideal scenario where predicted values should equal the true values. Each column represents the target coefficients in the true model, with each row corresponding to different models.

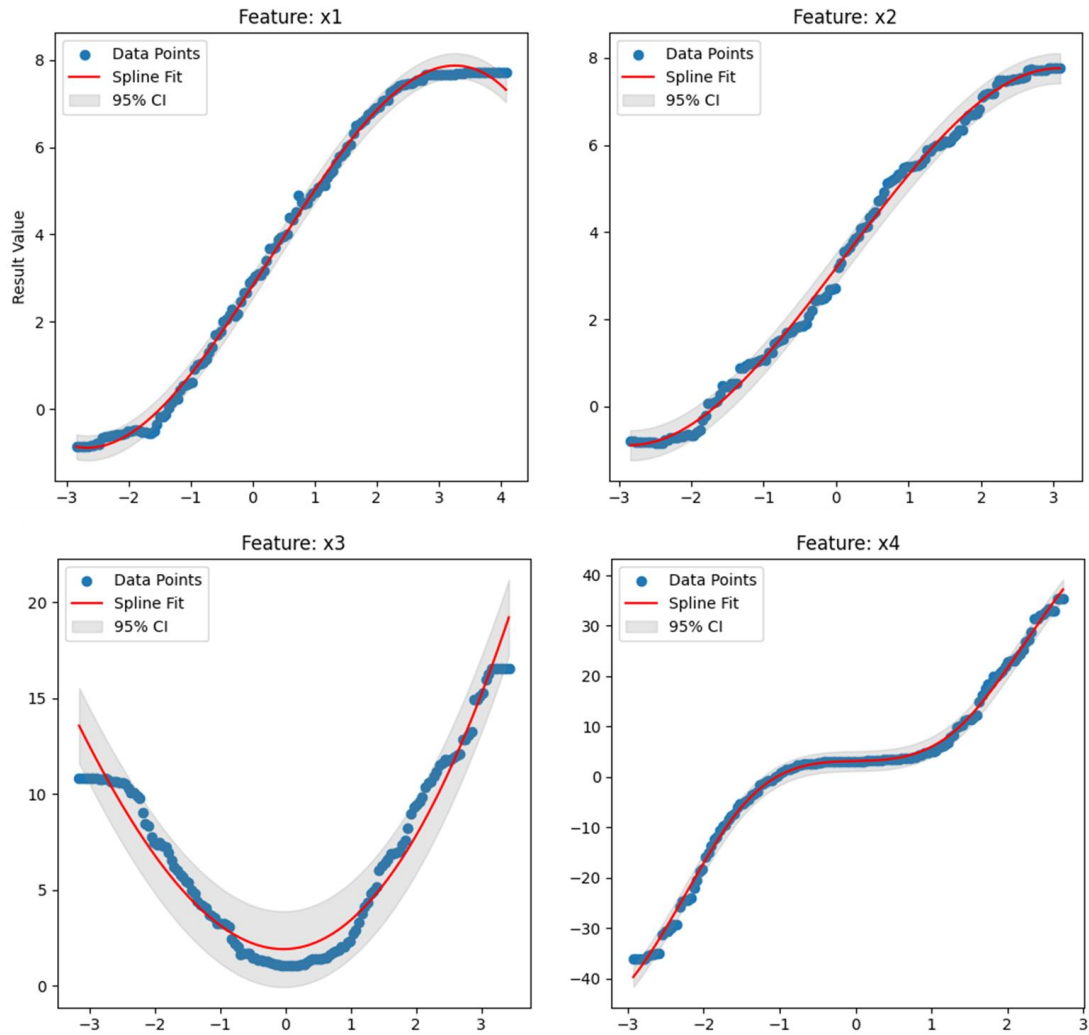


Figure 5: Partial dependence plot of explanatory variables.

## 4 Comparison of Spatial Weighting Scheme and ML Modes

### 4.1 Bandwidth Type and Spatial Weights Kernel Comparison

The evaluation of the accuracy of spatially varying coefficients, conducted using the GBR model across different bandwidths and spatial weight types, reveals consistent trends. Figure 6 illustrates that the correlation of SHAP values remains positive across bandwidths, yet exhibits a discernable threshold decline as bandwidth increases. The

influence of selecting different bandwidth types and weight methods on SHAP's spatial variability coefficient estimations appears minimal. In contrast, LIME's performance benefits significantly from adaptive bandwidth compared to fixed bandwidth, suggesting an insensitivity to the choice of bandwidth.

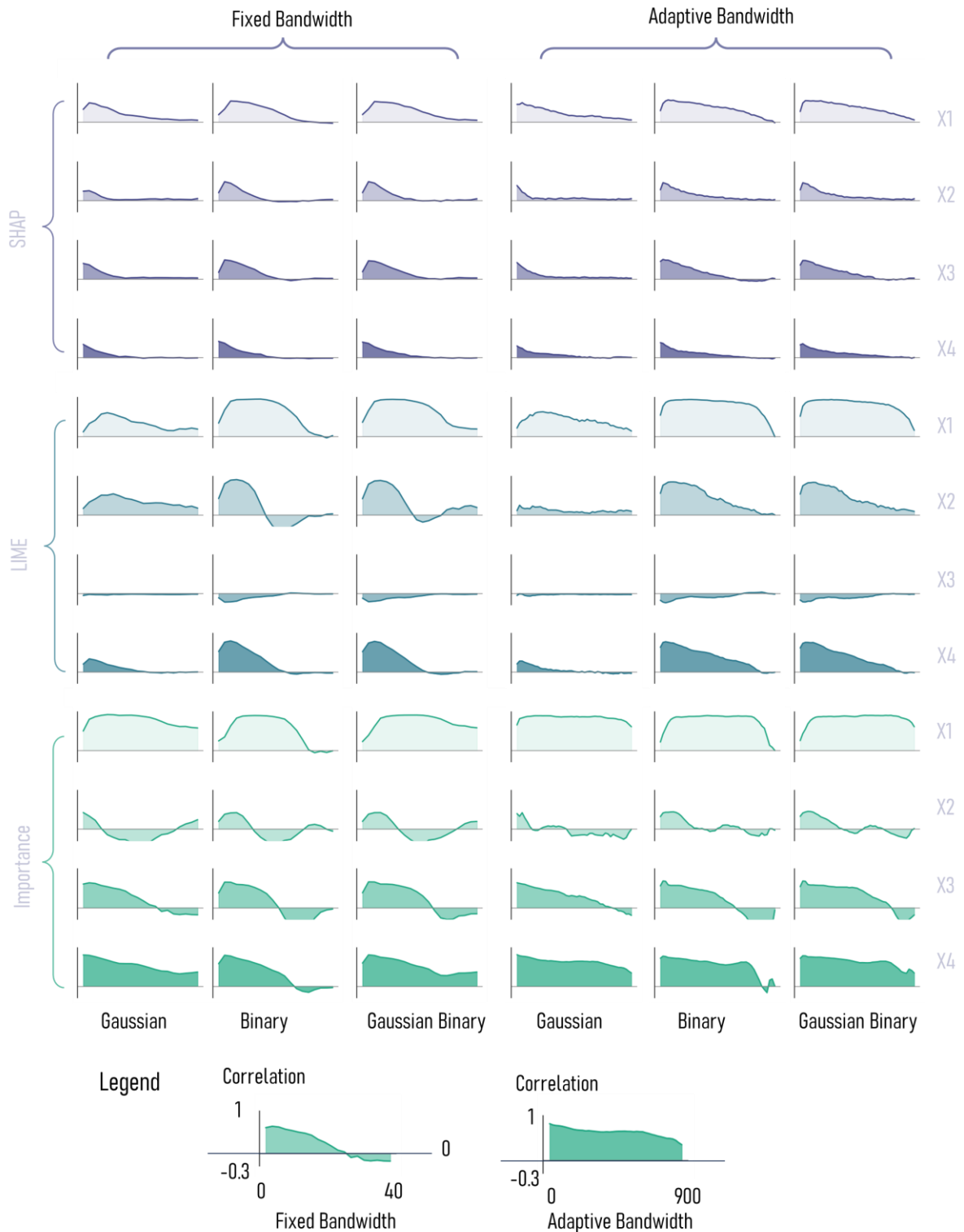




Figure 6: Model performance with different bandwidths and spatial weighting kernels. Each row illustrates how the correlation between the estimated spatial variability coefficients by the model and those of the actual model shifts with changing bandwidth. The X-axis specifies the bandwidth, while the Y-axis measures the correlation, spanning from -0.3 to 1. The graph includes a reference line at  $y=0$  to aid in visual comparison. For bandwidth settings on the X-axis, fixed bandwidth ranges from 2 to 40, indicating a more localized consideration of spatial data, whereas adaptive bandwidth extends from 20 to 900.

The Importance metric, notable for its higher accuracy, warrants detailed examination. The analysis across various bandwidth and spatial weight combinations reveals that the bandwidth size selection does not markedly affect the  $x_1$  variable, suggesting that linear spatial changes represent a global variable phenomenon. This pattern is similarly observed with the  $x_4$  variable. However, the Cosine spatial effect on the  $x_3$  variable shifts to negative beyond a certain bandwidth threshold, classifying it as a coefficient of mid-spatial scale variability. Among the different weighting methods, Gaussian weighting kernels exhibit the poorest performance, whereas Binary and Gaussian binary weights demonstrate more stability. This stability is especially apparent in the variability graph of the  $x_4$  variable under the Importance metric. The heatmap in Figure 7 further underscores that adaptive bandwidth provides a more robust adaptability to bandwidth changes, indicating that the Gaussian binary choice may offer a more stable option in XGeoML models.

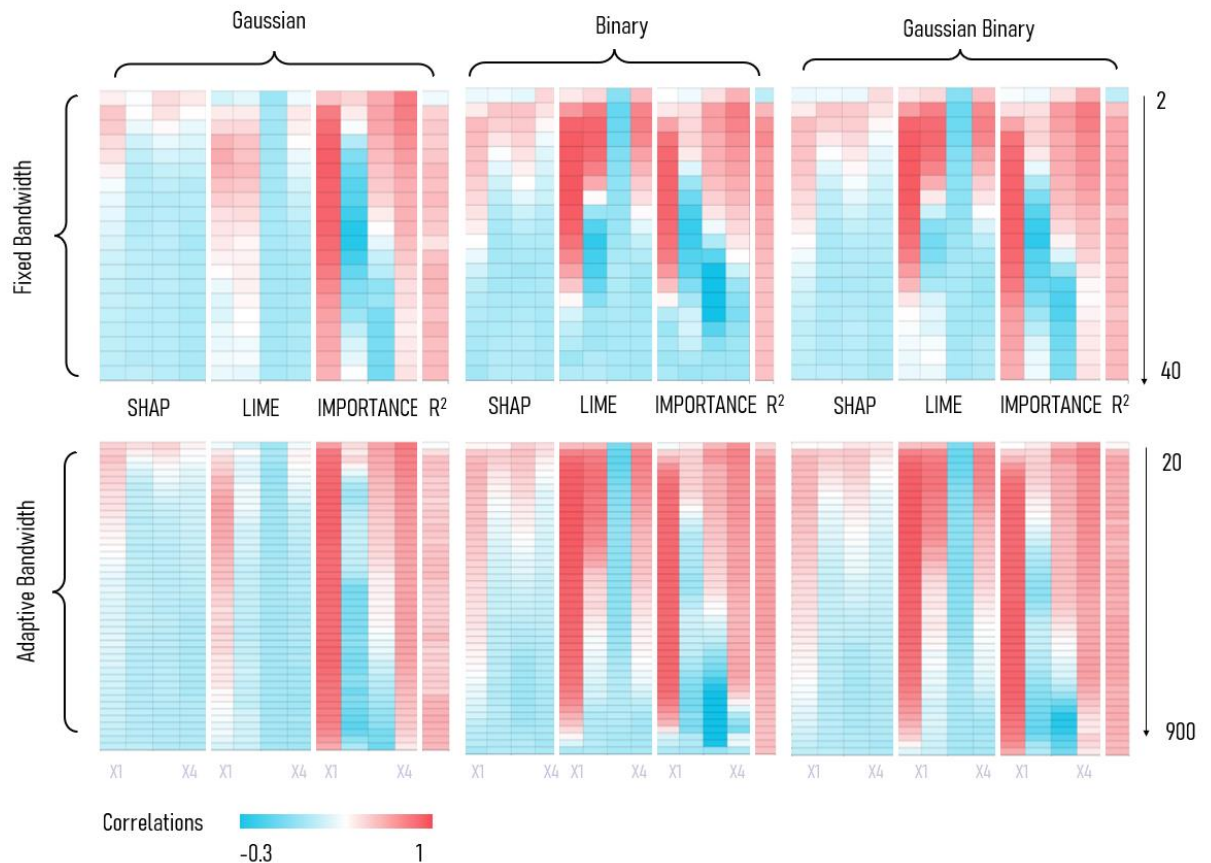


Figure 7 Correlation Heatmap across Various Bandwidth Types and Spatial Weighting Schemes. This heatmap is organized into six panels based on a combination of three spatial weighting methods—Gaussian, Binary, and Gaussian Binary—and two bandwidth types: Adaptive and Fixed. Each panel presents the correlation values for explanatory variables, utilizing SHAP, LIME, and Feature Importance, with the final column dedicated to the  $R^2$  values.

#### 4.2 Optimizing Model Selection by Balancing Performance, Efficiency, and Accuracy

This session evaluated and juxtaposed the efficacy of 29 regression models with the same Adaptive Binary spatial weighting scheme, encompassing ensemble techniques (such as Extra Trees and Random Forest), tree-based models, nearest neighbors methods, neural networks, SVMs, and linear models in Machine learning models. Figure 8 illustrates the performance of these models under varying bandwidth conditions, while Table 1S compiles their evaluation based on essential metrics like the

coefficient of determination ( $R^2$ ), execution time, and average correlation. The results revealed that the ExtraTreesRegressor emerged as the top-performing model in terms of data fitting, achieving an  $R^2$  value of 0.765 with a bandwidth of 180. However, its comparatively longer execution time highlights the crucial need for a trade-off between performance and computational efficiency during model selection.

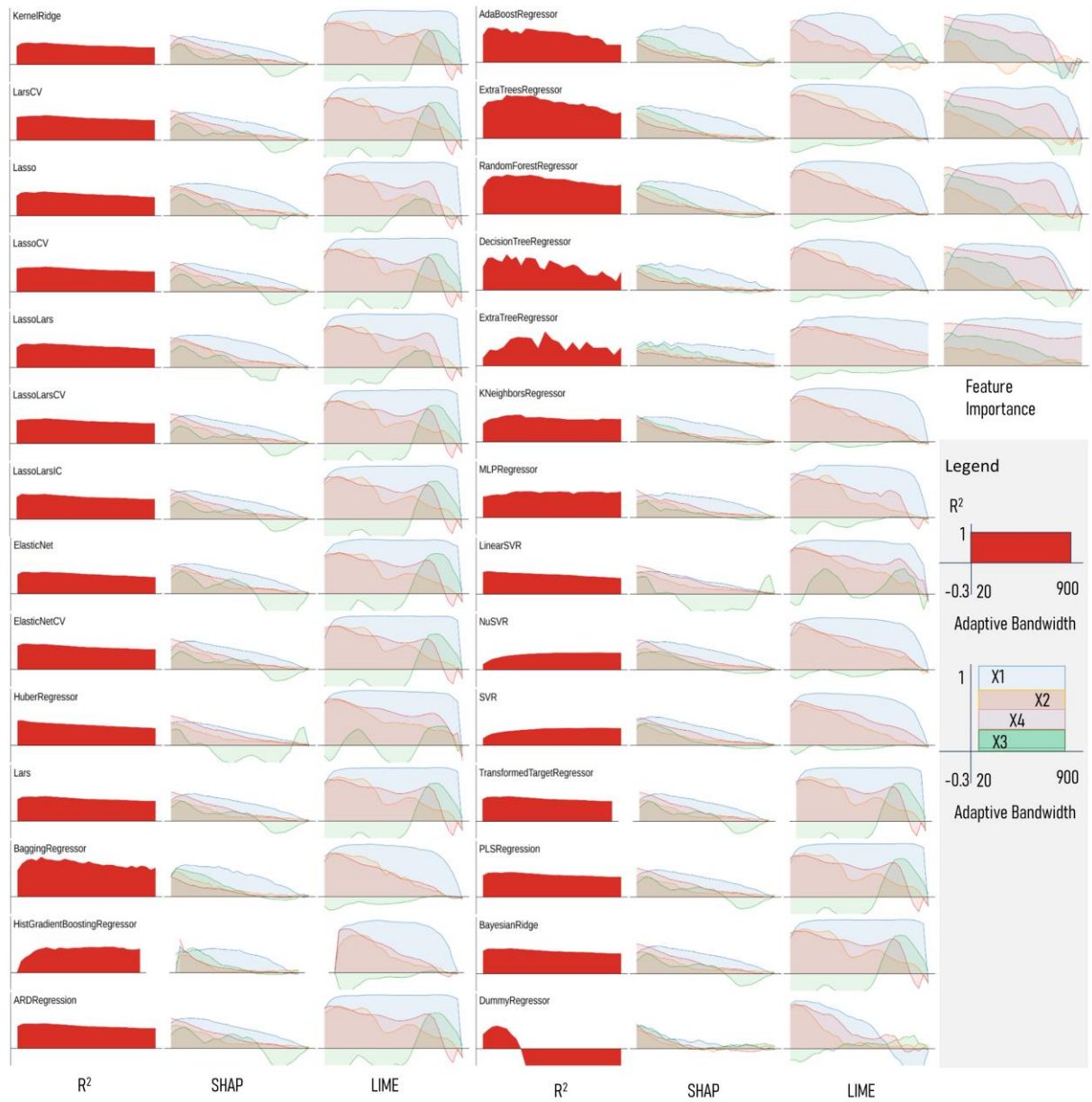


Figure 8: 28 XGeoML models' performance with the changing bandwidth. The X-axis specifies the bandwidth, while the Y-axis measures the correlation, spanning from -0.3 to 1. The graph includes a reference line at  $y=0$  to aid in visual comparison. For bandwidth settings on the X-axis, the adaptive bandwidth extends from 20 to 900.

While ensemble methods like Extra Trees and Random Forest showed superior performance, their longer runtime may not be suitable for applications requiring fast response times. Conversely, although linear models did not achieve the highest  $R^2$  values, their consistent performance and shorter runtime make them a reliable choice for situations demanding quick model responses. Notably, the Gaussian Process performed almost inadequately on our dataset (with an  $R^2$  value close to 0), indicating a possible mismatch with the data characteristics or a need for more precise parameter tuning. Similarly, the performance of Support Vector Machines (SVM) in this study was subpar, especially in terms of  $R^2$  values, suggesting that these models might not be the best option for handling such data.

Furthermore, we observed a relationship between the average correlation of spatial varying coefficients and the model accuracy. Models with higher  $R^2$  values not only demonstrated excellent fitting capabilities but also showed higher average correlations, indicating a strong relationship between predicted and actual values. This finding further reinforces the advantage of these models in terms of data fitting. However, some models, like the Histogram Gradient Boosting, despite having commendable  $R^2$  values, exhibited very low average correlations, revealing that a high  $R^2$  value does not necessarily imply high correlation, emphasizing the importance of considering multiple metrics when evaluating model performance.

This comparison highlights the imperative of contemplating various aspects, such as model fitting capability, computational efficiency, and data correlation, in the selection of models for a particular dataset. These insights lay a solid empirical foundation for data science professionals in employing XGeoML models, aiming to strike an optimal balance between performance and efficiency in specified application scenarios.

Table 2. XGeoML Model performance comparison

Model name	Model type	Runtime	R2	Average Correlation	Optimal Bandwidth
ExtraTreesRegressor	Ensemble	6043	0.765	0.631	180
BaggingRegressor	Ensemble	1498	0.707	0.366	180
RandomForestRegressor	Ensemble	8720	0.701	0.637	180
DecisionTreeRegressor	Tree	386	0.630	0.595	180
AdaBoostRegressor	Ensemble	3244	0.616	0.619	90
ExtraTreeRegressor	Tree	348	0.607	0.523	300
KNeighborsRegressor	Neighbors	972	0.476	0.255	270
MLPRegressor	Neural Network	8788	0.466	0.239	300
HistGradientBoostingRegressor	Ensemble	5690	0.456	0.072	660
ElasticNetCV	Linear	1733	0.454	0.427	90
LassoLarsIC	Linear	347	0.446	0.413	60
BayesianRidge	Linear	386	0.445	0.317	210
HuberRegressor	Linear	425	0.443	0.400	60
LarsCV	Linear	509	0.443	0.310	210
LassoLarsCV	Linear	455	0.443	0.310	210
LassoCV	Linear	1516	0.443	0.312	210
Lars	Linear	351	0.442	0.316	210
TransformedTargetRegressor	Compose	313	0.442	0.316	210
ARDRegression	Linear	441	0.442	0.336	210
PLSRegression	Cross_Decomposition	316	0.442	0.316	210
Lasso	Linear	321	0.426	0.390	210
LassoLars	Linear	317	0.426	0.390	210
DummyRegressor	Dummy	3364	0.408	0.292	120

LinearSVR	SVM	317	0.404	0.394	60
ElasticNet	Linear	409	0.385	0.453	90
KernelRidge	Kernel Ridge	549	0.384	0.306	210
SVR	SVM	5298	0.308	0.036	780
NuSVR	SVM	3164	0.306	0.053	750
GaussianProcessRegressor	Gaussian Process	236	0.005	0.168	180

## 5 Discussion and Conclusion

In this study, we introduce a novel integrated framework aimed at overcoming the challenges posed by the complexity of spatial data and potential nonlinear relationships, which limit the improvement of interpretability with traditional spatial analysis methods. we propose the Explainable Geospatial Machine Learning (XGeoML) model which enhances the ability to capture and explain spatial variability by continuing the local spatial weighting method of GWR and integrating machine learning regression and classification methods, along with explainable artificial intelligence (XAI) technology. The XGeoML model demonstrates its effectiveness through multi-model testing on synthetic datasets, showcasing its superior capability to accurately capture and explain spatial varying effects.

Our findings reveal that XGeoML models accurately capture the variation patterns of explanatory variables, notably the interactive effect of quadratic function and cosine spatial effect, while MGWR, GWR and GeoShapley Failed. It shows that the local spatial weighting can work for general machine learning models[11], and it further verified that Feature importance can provide a stable explanation for spatial varying effect [31]. This precision in capturing the dynamics of spatial data variability highlights the robustness of XGeoML in spatial analysis. However, the noise of SHAP

still prevent the capturing the spatial varying effect, which is the same to GeoShapley[40]. Moreover, the comparison prediction accuracy, the correlation between spatial varying coefficients and the actual model, and the performance of XGeoML under different bandwidth forms and weighting methods show their potential to understand the structure and dynamics inherent in spatial data.

Despite these advancements, the XGeoML model presents areas for improvement and opens avenues for future research. One limitation lies in the model's computational efficiency, particularly when handling large datasets or requiring real-time analysis. The balance between model complexity and computational demand necessitates optimization to ensure broader applicability and faster processing times. Moreover, the challenge of selecting optimal bandwidth and kernel types remains. The impact of these choices on model performance underscores the need for more adaptive and data-driven methods to determine these parameters, potentially through automated tuning processes or machine learning algorithms.

## Reference

1. Hammer, M.S., et al., *Effects of COVID-19 lockdowns on fine particulate matter concentrations*. Sci Adv, 2021. **7**(26): p. eabg7670.
2. Chaves, L.F., et al., *Snakebites are associated with poverty, weather fluctuations, and El Nino*. Sci Adv, 2015. **1**(8): p. e1500249.
3. Liu, L.B., et al., *Multiscale Effects of Multimodal Public Facilities Accessibility on Housing Prices Based on MGWR: A Case Study of Wuhan, China*. Isprs International Journal of Geo-Information, 2022. **11**(1).
4. Brunsdon, C., S. Fotheringham, and M. Charlton, *Geographically weighted regression*. Journal of the Royal Statistical Society: Series D (The Statistician), 1998. **47**(3): p. 431-443.
5. De Sabbata, S., et al., *GeoAI in urban analytics*. 2023, Taylor & Francis. p. 2455-2463.
6. Oshan, T.M. and A.S. Fotheringham, *A comparison of spatially varying regression coefficient estimates using geographically weighted and spatial-filter-based techniques*. Geographical Analysis, 2018. **50**(1): p. 53-75.
7. Griffith, D., *Spatial autocorrelation and spatial filtering*. 2003, Springer Berlin, Germany.

8. Gorr, W.L. and A.M. Olligschlaeger, *Weighted spatial adaptive filtering: Monte Carlo studies and application to illicit drug market modeling*. Geographical Analysis, 1994. **26**(1): p. 67-87.
9. Oshan, T.M., et al., *A scoping review on the multiplicity of scale in spatial analysis*. Journal of Geographical Systems, 2022. **24**(3): p. 293-324.
10. Murakami, D., et al., *Scalable GWR: A linear-time algorithm for large-scale geographically weighted regression with polynomial kernels*. Annals of the American Association of Geographers, 2020. **111**(2): p. 459-480.
11. Fotheringham, A.S., W. Yang, and W. Kang, *Multiscale geographically weighted regression (MGWR)*. Annals of the American Association of Geographers, 2017. **107**(6): p. 1247-1265.
12. Wheeler, D.C., *Simultaneous coefficient penalization and model selection in geographically weighted regression: the geographically weighted lasso*. Environment and planning A, 2009. **41**(3): p. 722-742.
13. Comber, A. and P. Harris, *Geographically weighted elastic net logistic regression*. Journal of Geographical Systems, 2018. **20**(4): p. 317-341.
14. Atkinson, P.M., et al., *Exploring the relations between riverbank erosion and geomorphological controls using geographically weighted logistic regression*. Geographical Analysis, 2003. **35**(1): p. 58-82.
15. Paez, A., *Exploring contextual variations in land use and transport analysis using a probit model with geographical weights*. Journal of Transport Geography, 2006. **14**(3): p. 167-176.
16. Brunsdon, C., S. Fotheringham, and M. Charlton, *Geographically weighted discriminant analysis*. Geographical Analysis, 2007. **39**(4): p. 376-396.
17. Jiang, Z., et al. *Learning spatial decision tree for geographical classification: a summary of results*. in *Proceedings of the 20th International Conference on Advances in Geographic Information Systems*. 2012.
18. Du, Z., et al., *Geographically neural network weighted regression for the accurate estimation of spatial non-stationarity*. International Journal of Geographical Information Science, 2020. **34**(7): p. 1353-1377.
19. Zhu, D., et al., *Understanding place characteristics in geographic contexts through graph convolutional neural networks*. Annals of the American Association of Geographers, 2020. **110**(2): p. 408-420.
20. Zhu, D., et al., *Spatial regression graph convolutional neural networks: A deep learning paradigm for spatial multivariate distributions*. GeoInformatica, 2022. **26**(4): p. 645-676.
21. Dai, Z., et al., *Geographically convolutional neural network weighted regression: A method for modeling spatially non-stationary relationships based on a global spatial proximity grid*. International Journal of Geographical Information Science, 2022. **36**(11): p. 2248-2269.
22. Mai, G., et al., *A review of location encoding for GeoAI: methods and applications*. International Journal of Geographical Information Science, 2022. **36**(4): p. 639-673.
23. Li, W., *GeoAI and deep learning*. The International Encyclopedia of Geography.,



- 2021.
24. Gao, S., *Geospatial artificial intelligence (GeoAI)*. 2021: Oxford University Press New York.
  25. Li, W. and C.-Y. Hsu, *GeoAI for large-scale image analysis and machine vision: Recent progress of artificial intelligence in geography*. ISPRS International Journal of Geo-Information, 2022. **11**(7): p. 385.
  26. Liu, P. and F. Biljecki, *A review of spatially-explicit GeoAI applications in Urban Geography*. International Journal of Applied Earth Observation and Geoinformation, 2022. **112**: p. 102936.
  27. Yang, W., et al., *Geographically weighted regression with the integration of machine learning for spatial prediction*. Journal of Geographical Systems, 2023. **25**(2): p. 213-236.
  28. Hagenauer, J. and M. Helbich, *A geographically weighted artificial neural network*. International Journal of Geographical Information Science, 2022. **36**(2): p. 215-235.
  29. Deng, M., W. Yang, and Q. Liu, *Geographically weighted extreme learning machine: A method for space-time prediction*. Geographical Analysis, 2017. **49**(4): p. 433-450.
  30. Georganos, S., et al., *Geographical random forests: a spatial extension of the random forest algorithm to address spatial heterogeneity in remote sensing and population modelling*. Geocarto International, 2021. **36**(2): p. 121-136.
  31. Grekousis, G., et al., *Ranking the importance of demographic, socioeconomic, and underlying health factors on US COVID-19 deaths: A geographical random forest approach*. Health & Place, 2022. **74**: p. 102744.
  32. Feng, L., et al., *Geographically and temporally weighted neural network for winter wheat yield prediction*. Remote Sensing of Environment, 2021. **262**: p. 112514.
  33. Wu, S., et al., *Geographically and temporally neural network weighted regression for modeling spatiotemporal non-stationary relationships*. International Journal of Geographical Information Science, 2021. **35**(3): p. 582-608.
  34. Kedron, P., T.D. Hoffman, and S. Bardin, *Reproducibility and Replicability in GeoAI*, in *Handbook of Geospatial Artificial Intelligence*. 2023, CRC Press. p. 369-387.
  35. Ribeiro, M.T., S. Singh, and C. Guestrin. "Why should i trust you?" *Explaining the predictions of any classifier*. in *Proceedings of the 22nd ACM SIGKDD international conference on knowledge discovery and data mining*. 2016.
  36. Lundberg, S.M. and S.-I. Lee, *A unified approach to interpreting model predictions*. Advances in neural information processing systems, 2017. **30**.
  37. Breiman, L., *Random forests*. Machine learning, 2001. **45**: p. 5-32.
  38. Masrur, A., et al., *Interpretable machine learning for analysing heterogeneous drivers of geographic events in space-time*. International Journal of Geographical Information Science, 2022. **36**(4): p. 692-719.
  39. Liu, P., Y. Zhang, and F. Biljecki, *Explainable spatially explicit geospatial*

*artificial intelligence in urban analytics*. Environment and Planning B: Urban Analytics and City Science, 2023: p. 23998083231204689.

40. Li, Z., *Extracting spatial effects from machine learning model using local interpretation method: An example of SHAP and XGBoost*. Computers, Environment and Urban Systems, 2022. **96**: p. 101845.